Journal of Non-Crystalline Solids 559 (2021) 120702

Contents lists available at ScienceDirect

Journal of Non-Crystalline Solids

journal homepage: www.elsevier.com/locate/jnoncrysol

Influence of Ag nano particles on spectroscopic and luminescence properties of Dy^{3+} doped borate glasses

Ashok Ande [a], J. Bhemarajam [a], Venkanna Kanneboina [b], Swapna [a], M. Prasad [a,*]

[a] Department of Physics, Osmania University, Hyderabad-500007, Telangana, India
[b] Department of Physics, Indian Institute of Technology Guwahati, 781039, Assam, India

ARTICLE INFO

Keywords:
Silver nanoparticles
Absorption spectra
Raman spectra
LSPR
Photoluminescence

ABSTRACT

Dy^{3+} doped lithium zinc borate glasses with silver (Ag) nanoparticles (NPs) were synthesized by the conventional melt quenching method. Impact of silver NPs on the luminescence properties of $59B_2O_3$: 20ZnO: $10Na_2O$: $10Li_2O$: 0.5SnO: $0.5Dy_2O_3$ glasses doped with Dy^{3+}ions were investigated. Ag^+ ions have been reduced and nucleated to AgNPs by thermochemical redox method. Amorphous characteristics of the glasses were confirmed by XRD measurements. Raman and Fourier transform infrared spectra were used to estimate structural and vibrational bands of the glass samples. Localized surface plasmon resonance (LSPR) band is observed at 419 nm for 0.3 mol% of Ag along with three absorption bands of dysprosium were observed. Luminescence studies were performed on these glasses and found that three emission bands at 484, 575, and 665 nm when excited with wavelength of 349 nm, which corresponds to $^4F_{9/2}$ to $^6H_{15/2}$, $^4F_{9/2}$ to $^6H_{13/2}$, and $^4F_{9/2}$ to $^6H_{11/2}$ transitions of Dy^{3+} ions.

1. Introduction

Many of the research groups have shown great interest in the rare earth ions (RE) and metallic nanoparticles (NPs) co-embedding in suitable glassy matrices for enhancing the luminescence properties. These types of amorphous materials with a combination of RE and NPs having nanostructures are gaining huge attention in recent years [1–9]. These materials have potential applications in various fields such as display technology, information processing, solid-state lasers, fiber communication, planar waveguides [10–12], etc. RE ion-doped borate glasses deliver such types of significant potential applications due to low melting point (MP), higher thermal stability factor (TSF), better thermal soluble nature, a different type of coordination number [13]. They are good host matrices among other glasses due to boric oxide plays an important role as glass forming and flux material [14]. Dy^{3+} rare-earth ions exhibit good luminescent properties and emit blue, yellow emissions. Interestingly, these Dy^{3+} ions doped glass systems also emits white light by excitation of blue or ultraviolet wavelength [15].

Glass system exhibits surface plasmon resonance phenomenon by the resonance of incident frequency of electromagnetic radiation with a frequency of electronic oscillation. It is accounted that rare-earth ions have been excited by the recombination of photo-generated energy carriers in nanostructured materials and then subsequently, transfers the energy to rare-earthed ions in nanomaterials. It is also observed that Raman scattering and luminescence properties have been improved by adsorbed molecules on the rough metal surfaces [16,17]. This is supported the investigations on the optical properties of composites material, like Dy^{3+} doped glasses contained Ag NPs. In this glass system any significant impact of the metallic particles on the absorption and emission rates of the RE ions should be the priority role of electronic origin. The electro-magnetic interactions were observed at Mie resonance frequencies due to the higher field gradient close by metallic particles. In order to fabricate devices with improved optical properties, luminescence quenching should be minimized by decreasing the concentration of RE ions [18–20]. In this way, efficiency of luminescence of glass containing metallic nanoparticles that are doped by a small amounts of rare earth ions have improved due to huge local electric field present on the ions situated close to the NPs [2].

In the present study, Dy^{3+} doped B_2O_3-ZnO—Na_2O-Li_2O-SnO glasses containing silver nanoparticles were investigated. Structural properties were studied by Raman spectra, FTIR spectra, XRD measurements, and composition analysis studied by SEM measurements. Furthermore, the LSPR band from the optical absorption, enhanced luminescence characteristics of borate glasses containing silver nanoparticles were

* Corresponding author.
E-mail address: prasad5336@yahoo.co.in (M. Prasad).

https://doi.org/10.1016/j.jnoncrysol.2021.120702
Received 7 November 2020; Received in revised form 26 January 2021; Accepted 27 January 2021
Available online 5 February 2021

investigated.

2. Experimental details

The glass samples with composition of (60-x-y-z) B_2O_3 – 20 ZnO – 10 Na_2O – 10 Li_2O – x SnO – y Dy_2O_3 – z Ag_2O (where $x = 0.5\%$, $y = 0.5\%$, $z = 0.05$, 0.1, 0.3, 0.5, 1%) have been synthesized by the conventional melt quenching method. These glasses were prepared in the compositional ratios and as shown in Table 1. The -borate glasses were prepared using chemicals such as H_3BO_3 (99.9%) (B_2O_3), ZnO (99%), Na_2O (99.9%), Li_2O (99.9%), Dy_2O_3 (99.9%), SnO (99.9%), Ag_2O (99.9%). Initially the chemicals were properly weighted and mixed in an agate mortar to attain uniform nature. Then well-mixed powders were put into the porcelain crucible and kept inside the pre-heated electrical furnace in range of 900–1050 °C for 1 h. The molten liquid combination of the mixture has been quenched by slowly dropping on pre-heated stainless-steel mold at one-third of the melting temperature and afterward annealed at 300 °C for 5 h to eliminate the thermal as well as mechanical strains. Structural properties of annealed synthesized glasses were studied by XRD Philips PW (1140) diffractometer with CuK_α radiation. The XRD measurements were done on the bulk samples at room temperature in the 2θ range of 10–70° with step size of 0.02°, scan step time of 0.2 s, voltage of 40 KV and current of 30 mA of CuK_α X-ray source was used. The Scanning Electron Microscope (SEM) and Energy Dispersive Spectroscopy (EDS) images of samples were recorded with an EDS OXFORD spectrometer. The samples for SEM measurements were prepared as mentioned in the experimental details section. The back side of the prepared samples were fixed on the SEM sample holder (stub) with carbon tape and then gold particles were sputtered on the front side of the samples for few seconds. These samples were loaded in SEM chamber for measurements. The voltage of 10 KV and current of 200 A was used for SEM measurements. Differential Scanning Calorimetry (DSC) (DSC Q-20) has been used to measure the characteristic temperature of the BDAg parent sample. DSC measurements were performed on the samples in the temperature range of 200–750 °C with temperature rate of 10 °C/min in the environment of Nitrogen gas flow of 50 ml/min. The mass of the sample is 2.351 mg. The UV–Vis-NIR spectrometer (Shimadzu UV-3100) was used to record the optical absorption spectra at room temperature in the wavelength range of 250–1350 nm. Infrared absorption studies were investigated by the FTIR spectrometer (Perkin Elmer, model: 1605) using KBr pallets in the range of 1600 - 400 cm^{-1}. The Raman spectra of glass matrix was recorded with a micro-Raman spectrometer (LABRAM-HR) in the wavenumber range of 200–1000 nm using Ar ion laser with excitation wavelength of 633 nm.

2.1. Synthesis and mechanism of the nanoparticles by thermo-chemical reduction method

The glass matrix B_2O_3-ZnO—Na_2O-Li_2O-SnO-Dy_2O_3 with Ag_2O ($AgNO_3$) was prepared at 1000 °C of melting temperature. Different concentrations of 0.05, 0.1, 0.3, 0.5, 1 mole% of Ag_2O were chosen and SnO was used as selective reduction agent. The reduction agent SnO reacts with the Ag^+ and it converts the silver ions into silver nanoparticles as $Ag^+ \rightarrow Ag^\circ$.

The NPs growth takes place during the heat-treatment at 420 °C for 5 h, because at this temperature the material viscosity is sufficient to support the Ag^+ diffusion. The arrangement of neutral silver atoms (Ag^o) is represented by the following reaction:

$$Ag^+ + e^- \rightarrow Ag^o$$

The probable mechanism is Ag^+ to Ag^o by selective thermo-chemical reduction method. Reduction agent SnO reduces the Ag^+ ions into Ag NPs as well as Sn^{2+} into Sn^{4+} respectively. The feasible spontaneous reduction reaction is

$$Sn^{2+} + 2\,Ag^+ \rightarrow Sn^{4+} + 2\,Ag^\circ$$

Glasses with presence of Ag_2O is post annealed at 500 °C for 5 h from the average temperature of glass transition temperature (T_g) at 441 °C and onset crystallization temperature (T_o) at 565 °C.

Table 1
Compositions of various reduced agents of BDAg glass systems (mol%).

Sample code	B_2O_3	ZnO	Na_2O	Li_2O	SnO	Dy_2O_3	Ag_2O
BDAg-0.05	58.95	20	10	10	0.5	0.5	0.05
BDAg-0.1	58.9	20	10	10	0.5	0.5	0.1
BDAg-0.3	58.7	20	10	10	0.5	0.5	0.3
BDAg-0.5	58.5	20	10	10	0.5	0.5	0.5
BDAg-1	58	20	10	10	0.5	0.5	1

3. Physical properties

3.1. Density estimation

The density of prepared samples is estimated through standard Archimedes principle (Eq. (1)). Xylene was used as an immersive fluids and measurements of all glass samples were done at room temperature.

$$\rho = \left[\frac{a}{a-b}\right]\rho_x \tag{1}$$

Where a, b is the weight of the glasses in air and xylene respectively. The standard density value of xylene at room temperature is 0.865 g/cm^3. Increment of density is attributed to the changes in the structure of glass network due to the transformation of triangular units of $[BO_3]^{3-}$ into tetrahedral units of BO^{4-} and increment of molecular mass [21]. Consequently, the molar volume of the sample estimated from density, using below equation:

$$V_m = \frac{M_i x_i}{\rho} \tag{2}$$

Where V_m is the molar volume, M_i and x_i are the molar mass and content of i-oxide in the glass, ρ is the density of each sample. The values of the molar volume are listed in Table 2. It is observed that there is a decrement in molar volume with increment in density when the increase in the concentration of Ag NPs in the composition. Oxygen packing density (OPD) of all samples is estimated from the density values by using the Eq. (3)

$$\text{OPD} = \left(\frac{\rho}{\text{M}}\right)\text{x}\ O_n \tag{3}$$

Where O_n is the number of oxygen atoms and M is the molecular weight. The respective molar volume (V_m) and OPD values are given in Table 2.

3.2. Ion concentration

The ion concentration in borate glasses was estimated by Eq. (4).

$$N = \frac{X\%\ x\ p\ x\ N_A}{\text{M}}\ ions\ cm^{-3} \tag{4}$$

Here, X% is mole percentage of dopants, ρ is the density of glasses, N_A is the Avogadro number. Consequently, calculated the polar radius, intermolecular distance, and field strength parameters using the following equations based on the ions concentration [22].

3.3. a. Polaron radius

$$r_p\ (\text{Å}) = \frac{1}{2}\left(\frac{\pi}{6N}\right)^{1/3} \tag{5}$$

Table 2
Physical and optical parameters of Dy^{3+} doped Ag NPs of BDAg glass system.

Sample code	Density (ρ) (g/cm^3)	Molar volume (V_m) (cm^3/mol)	Oxygen packing density (O.P.D) (mol/l)	Ion concentration (N x10^{22} ion/cm^3)	Polaron radius (r_p x 10^{-8} Å)	Inter – nuclear distance (r_p x 10^{-8} Å)	Field strength F * 10^{17} (cm^2)	Cutoff wavelength (nm)	Optical Band gap (E_{opt}) (eV)	Urbach EnergyΔE (eV)	Refractive Index (μ)
BDAg-0.05	3.30 ± 0.16	20.93 ± 1.05	104.56 ± 5.22	0.63 ± 0.03	2.17 ± 0.11	5.39 ± 0.30	335.83 ± 16.8	356	4.02	0.13	2.17
BDAg-0.1	3.30 ± 0.16	20.96 ± 1.05	104.37 ± 5.21	1.25 ± 0.06	1.73 ± 0.09	4.30 ± 0.22	527.55 ± 26.4	374	3.93	0.26	2.18
BDAg-0.3	3.29 ± 0.16	21.14 ± 1.06	103.29 ± 5.16	3.74 ± 0.19	1.20 ± 0.06	2.98 ± 0.15	1095.24 ± 54.8	388	4.22	0.25	2.13
BDAg-0.5	3.31 ± 0.16	21.08 ± 1.05	103.40 ± 5.17	6.29 ± 0.31	1.01 ± 0.05	2.51 ±.12	1545.70 ± 77.3	411	4.02	0.25	2.17
BDAg-1	3.34 ± 0.17	21.14 ± 1.06	102.64 ± 5.13	12.72 ± 0.64	1.60 ± 0.08	1.98 ± 0.10	1740.32 ± 87.0	428	3.92	0.26	2.12

3.4. b. Inter-nuclear distance

$$r_i\ (\text{Å}) = \left(\frac{1}{N}\right)^{1/3} \tag{6}$$

where N is ions concentration

3.5. c. Field strength

$$F = \frac{Z}{(r_p)^2} \tag{7}$$

Where Z is the atomic mass and r_p is the radius of polarons.

3.6. Optical absorption studies

The Urbach energy (ΔE), which indicates the disorderness in the amorphous materials. It is determined from the inverse of its slope, as given by [23]

$$\alpha(\upsilon) = \beta\exp\left(\frac{h\upsilon}{\Delta E}\right) \tag{8}$$

Where, β is a constant and ΔE is the width of the localized band tail states.

Direct ($m = ½$) and Indirect ($m = 2$) optical bandgaps are used by Mott and Davis formula [24].

$$\alpha(\omega) = \left(\frac{B(h\upsilon - E_{opt})^m}{h\upsilon}\right) \tag{9}$$

where E_{opt} is the optical energy band gap, hυ is the photon energy and B is band tailing parameter constant. The Refractive index (n) of each sample was estimated from the optical energy band gap through relative formula demonstrated by Dimitrov and Sakka [25] and given Table 2.

$$\frac{(n^2-1)}{(n^2+1)} = 1 - \left(\frac{E_g}{20}\right)^{\frac{1}{2}} \tag{10}$$

where E_g is the direct band gap and n is refractive index.

All the estimated physical parameters are given in Table 2. As the concentration of Ag_2O in the glass system increases, there are structural changes taking place and this causes the changes in the arrangement of atoms inside the glass network and conversion of BO_3 units into BO_4 units takes place as a result there is a variation in density and refractive index of the glass. Luminescence and optical properties have varied with composition of the glass matrix due to the variation in the concentrations of oxides, which make changes in molar volume, density and other physical properties of a glass system.

4. Results and discussion

4.1. X-ray diffraction

Fig. 1 indicates the XRD pattern of different concentrations of Ag of Dy^{3+} doped BDAg glass matrix. The XRD pattern was measured in the 2θ range of 10° to 70°. XRD analysis is used to determine the amorphous nature of the synthesized samples. It was found that the samples have shown a broad peak at 28° and 41°, which correspond to the glass matrix of samples [21,26]. No sharp peaks were absorbed for these samples. The presence of these broad peaks suggest that the amorphous nature of the glass samples [26]. Observed very low intensity peak around 33° could be due to the low concentration of Ag particles as compared with the bulk glass matrix. It is found that no other crystalline peaks were observed in the XRD pattern.

4.2. SEM and EDS analysis

SEM morphology of samples is shown in Fig. 2. SEM images explore the smooth surface of the samples with high uniformity and without any crystals. This smooth surface indicates the amorphous behavior of the glass system. Any grain boundaries were not observed in the surface morphological image of the host BDAg-0.05, BDAg-0.1, BDAg-0.3, BDAg-0.5, BDAg-1 glass samples, which are shown in Fig. 2 [27]. The observed clusters may be due to the sputtered gold particles during SEM measurements. The compositional analysis of the glasses was also studied by using the EDS technique. The EDS spectra of the BDAg glass system was shown in Fig. 3. Compositional elements of Borate (B), Zinc (Zn), Silver (Ag), Sodium (Na), Lithium (Li), Dysprosium (Dy), Tin (Sn) are found in the EDS spectra. Those results show that corresponding elements present in the respective glass matrices that were used at the time of preparing glass samples.

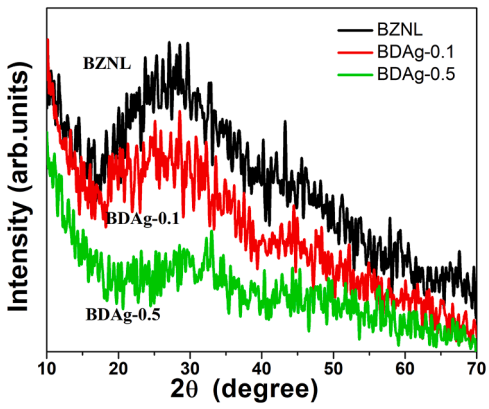

Fig. 1. XRD pattern of Dysprosium doped zinc borate glass system.

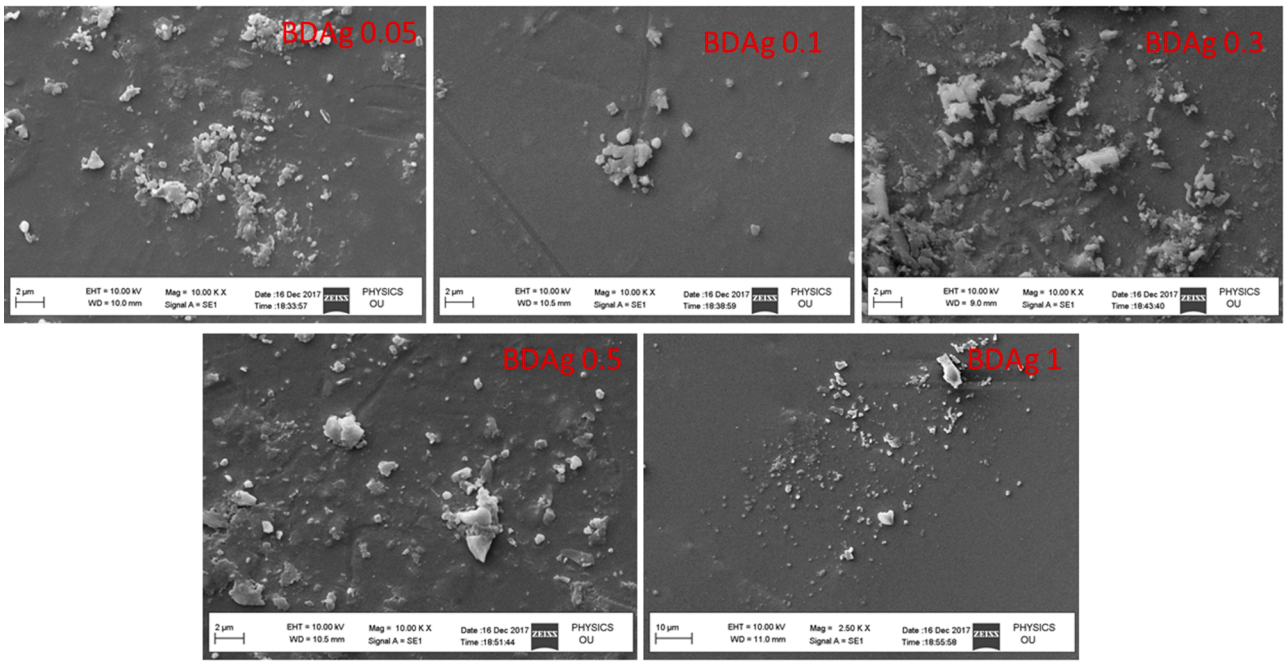

Fig. 2. SEM images of BDAg glass system.

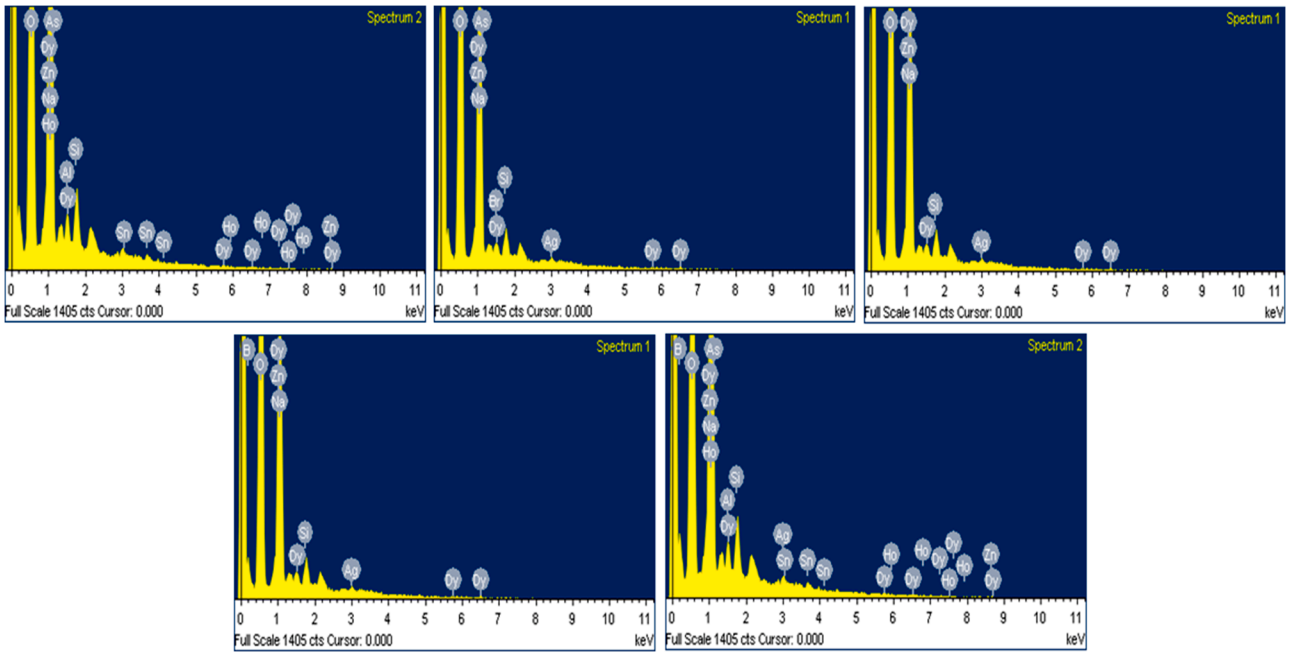

Fig. 3. EDS spectra of BDAg glass system.

4.3. DSC studies

Fig. 4 shows the DSC measurements of the zinc borate glass system. Characteristic temperatures of the glasses such as glass transition temperature (T_g), onset crystallization temperature (T_o), peak crystallization temperature (T_p), and melting temperature (T_m) were estimated from the DSC measurements. Estimated values are 441 °C, 565 °C, 594 °C, and 688 °C correspond to T_g, T_o, T_p, and T_m respectively. Therefore, the post-annealing temperature is selected to be at 500°C for 5 h. This annealing temperature is higher than the T_g, where the viscosity of the glass is suitable for the diffusion, aggression, and growth of silver nanoparticles [28]. Annealing was done slightly above the glass transition temperature; however, no crystalline peaks were observed, which is confirmed by XRD measurements.

The glass thermal stability factor (TSF) was calculated as $\Delta T = T_p - T_g = 153$ °C. Thermal stability of the glasses is described by $\Delta T > 100$ °C [29]. This glass stability factor indicates that the glass has greater thermal stability which suggests that the glass can be used as a prominent material for optical fibers. Our glass system is having the thermal stability for usage in fibers for telecommunications. So, it can be considered as a potential material for telecommunications industry. Hruby parameter indicates the stability of the glass, which is calculated as

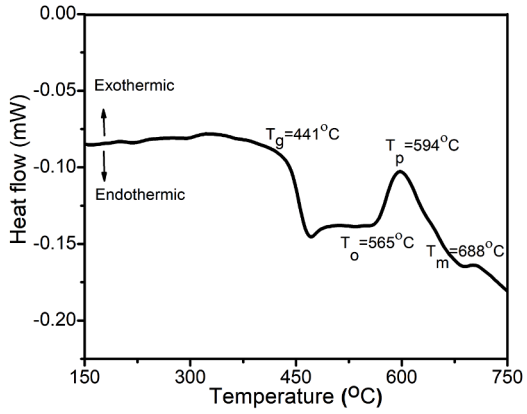

Fig. 4. DSC Thermogram of Dysprosium doped BDAg glass system.

$$Hr = \frac{Tp - Tg}{Tm - Tp} \tag{11}$$

Where H_r is used to measure the ability of the formation of the glasses. A higher value of H indicates the higher ability of the formation of glasses [30] i.e. The Hruby parameter calculated for the present glasses is Hr = 1.63 this suggests that these glasses possess higher glass forming ability.

4.4. UV–Vis-NIR spectroscopy studies

Fig. 5. shows the absorption spectra of Dy^{3+} doped Ag NPs of the BDAg glass matrix in the wavelength range of 250–1350 nm. Several absorption bands are observed for the samples in the range of 250–1350 nm due to transition from a lower energy ground states to higher energy excited states respectively [31]. It is observed that the growth of Ag nanoparticles has enhanced with an increase in Ag composition from 0.05 to 0.3 mol%. The absorption bands in the UV–Vis region at 396 nm and 411–420 nm correspond to $^6H_{15/2}$ to $^4I_{13/2}$, $^4F_{7/2}$, and $^6H_{15/2}$ to $^4G_{11/2}$ electronic transitions [32]. In Fig. 5, observed absorption bands in NIR region at 840–890, 911–936, 1080–1090,1257–1268 nm corresponds to $^6H_{15/2}$ to $^7F_{5/2}$, $^6H_{15/2}$ to $^6F_{7/2}$, $^6H_{15/2}$ to $^6F_{9/2}$, and $^6H_{15/2}$ to $^6F_{11/2}$ electronic transitions respectively [32]. These observed bands are tabulated in Table 3. Fig. 5 shows the strong absorption peak around 400 nm represent surface plasmon resonance (SPR) of Ag NPs in the samples. The luminescence properties have enhanced in the presence of the NPs, which is attributed to huge localized electric field in or near the area of rare earth ions. This process is induced by surface plasmon resonance of NPs. The electric field is increased to maximum value at particular separation of NPs [29,33]. The size of NPs has increased as the increase of Ag concentration from 0.05 to 0.3% by aggregation of NPs,

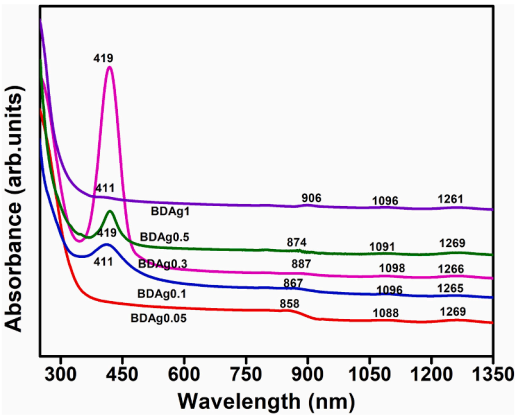

Fig. 5. Absorption spectra of BDAg glass system.

Table 3
Optical absorption spectra of Dy^{3+} doped BDAg glass system.

Composition (Sample codes)	Absorption band positions (nm)
BDAg-0.05	—- 858 1088 1269
BDAg-0.1	411 867 1096 1265
BDAg-0.3	419 887 1098 1266
BDAg-0.5	419 874 1091 1269
BDAg-1	411 906 1096 1261

which results in formation of the non-spherical particles. The growth of NPs is saturated and high intensity SPR band is observed at Ag of 0.3% (Fig. 5). Beyond Ag concentration of 0.3%, the intensity of SPR bands decreased as increase in the Ag concentration [29,33]. The possible reason is that the incorporation of silver as ion (Ag^+) into the glass network at higher Ag concentration and formation of metallic silver is reduced. This could be the reason for the decrease in the intensity of SPR band at 0.5 and 1% of Ag concentration compare to 0.3% of Ag.

4.5. Fourier transform infrared (FTIR) spectroscopy

Fig. 6. shows the FTIR absorption spectra of different concentrated Ag of Dy^{3+} doped (60-x-y-z) B_2O_3 – 20 ZnO – 10 Na_2O – 10 Li_2O – x SnO – y Dy_2O_3 – z Ag_2O glass matrix. FTIR spectra of samples were measured in the wavenumber range 1600–400 cm^{-1} at room temperature. FTIR band positions of the BDAg glass samples, their band positions and assigned vibrational bands are listed in Tables 4. For the BDAg glass matrix, it was observed that the prepared samples show different bands around 680–690 cm^{-1}, 920–1000 cm^{-1}, 1230–1250 cm^{-1}, and 1360–1380 cm^{-1} [21,26]. The observed band around 680- 690 cm^{-1} corresponds to the bending vibration of B-O and B-O-B modes in penta-borate groups. The band positions at 920–1000 cm^{-1} are ascribed to the symmetrical stretching mode of BO_4 units and it is attributed to metal and oxygen vibrations. It is observed that the bands are shifting towards higher wavenumber as the composition of the glass is varied. The bands are ascribed to 1230–1250 cm^{-1} related to stretching vibrations of B-O bond, vibrations of BO_4^- tetrahedra, symmetric stretching vibration of BO_3^- and B-O bridge the B_3O_6 rings and BO_3 triangles [21]. The FTIR results also supports the absorption spectra by shifting of the band position of glasses to lower wavenumber side from higher wavenumber at high concentration.

4.6. Raman spectroscopy

Raman spectra of Dy^{3+} doped (60-x-y-z) B_2O_3 – 20 ZnO – 10 Na_2O – 10 Li_2O – x SnO – y Dy_2O_3 – z Ag_2O glasses with different concentrations of Ag were shown in Fig. 7. The deconvoluted spectra of BDAg glass

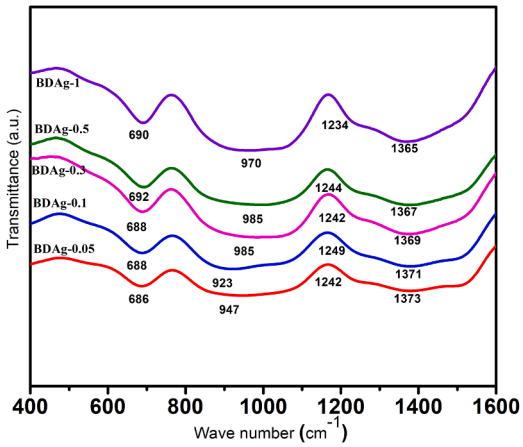

Fig. 6. FTIR spectra of BDAg glass system.

Table 4
FTIR band assignments of Dy3+ doped Ag NPs of BDAg glass system.

Wave number (cm^{-1})	Assignments
688	B-O bonds bending vibration and B-O-B bonds bending vibration from pentaborate groups
854–985	Symmetrical stretching vibration of BO_4 units
1255	B-O bond stretching vibrations and B-O bridging between B_3O_6 rings and BO_3 triangles, vibrations of pentaborate along with BO_4^- tetrahedral, pyroborate units, symmetric stretching vibration of BO_3^-
1344	Asymmetric stretching vibrations of B-O bond in trigonal BO_3 units from various types (meta,pyro,ortho,penta) of borate groups

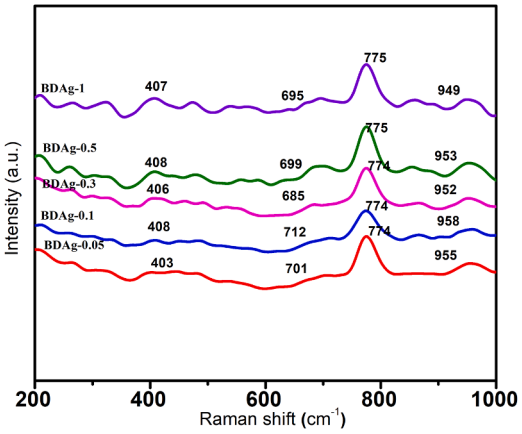

Fig. 7. Raman spectra of BDAg glass system.

system in the wavenumber range of 200–1000 cm^{-1} is shown in Fig. 8. Raman spectroscopy is used to study the presence of different structural units and the additional modifier ions of the glass matrix. The Raman spectra of the glass system are complementary to the FTIR spectrum. The peak positions and assignments of the Raman bands are tabulated in Table 5. Four major Raman bands are observed and the assigned Raman bands are in the following ranges: band 1: 403- 408 cm^{-1}, band 2: 685-712 cm^{-1}, band 3: ~774 cm^{-1} and band 4: 949- 958 cm^{-1} [34,35]. In case of lower frequency regions, the band 1 around 410 cm^{-1} is attributed to B-O-B of borate unit. The bands around 680–710 cm^{-1} corresponds to the chains and rings-type metaborate contained non-bridging oxygen (O) group. The band 3 ~774 cm^{-1} is due to vibrations of a six-membered rings containing both BO_3 and BO_4 [21,36]. The band around 950 cm^{-1} corresponds to the B-O stretching mode of tetrahedral

Table 5
Raman band assignments of Dy^{3+} doped Ag NPs of BDAg glass system.

Wave number (cm^{-1})	Assignments
~410	ring angle bending (B-O-B) from borate units
680–710	Chain and ring type metaborate containing non-bridging oxygen groups.
~774	ring breathing vibration of six membered ring contains both BO_3 triangles and BO_4 tetrahedral
950	B-O stretching mode of tetrahedral BO_4 in $B_3O_9^{3-}$ (orthoborate) units

BO_4 in $B_3O_9^{3-}$(orthoborate) units [34,35]. In the present glass matrix, it is found that several bands of glass matrix are observed in Raman deconvoluted spectra and these wider bands indicate amorphous nature of the glass system. Luminescence of the material varies with structural arrangement of atomic groups and concentration of the oxides present in the glass network. In this present glass system, as the Ag_2O concentration is increased, some of the bonds could be observed and rearranged, the BO_3 units are converted into BO_4 units. This also results in the formation of non-bridging oxygen (NBOs), this attributes to the variation in the intensity of emission bands.

4.7. Photoluminescence

Fig. 9 shows the photoluminescence emission spectra of Ag concentration of dysprosium ions doped BDAg glass system in the wavelength limit of 400–680 nm by excitation wavelength of 349 nm. Three distinct emission peaks were found at 484, 575 and 665 nm, which corresponds to $^4F_{9/2}$ to $^6H_{15/2}$, $^4F_{9/2}$ to $^6H_{13/2}$, and $^4F_{9/2}$ to $^6H_{11/2}$ transitions respectively [37]. It was observed that the position of the emission band has not changed, however, the intensity of the peaks has increased with increase in concentration of Ag from 0.05 to 1% in the Dy^{3+} doped BDAg glass matrix. These results are in good agreement with the previously published research on Dy^{3+} doped glasses [13,21,38]. The most intense emission is observed for $^4F_{9/2}$ to $^6H_{13/2}$ (yellow) transitions at 575 nm and followed the $^4F_{9/2}$ to $^6H_{15/2}$ (blue) transitions at 484 nm. Whereas a small intensity band is observed for $^4F_{9/2}$ to $^6H_{11/2}$ transition at 665 nm. The high intensity of the emission band at 575 nm due to electric dipole transition and it is hypersensitive transition as it follows the selection rules $\Delta L = \pm 2$ and $\Delta J = \pm 2$ for transitions and it is very sensitive to the environment of rare earth ions [34,39–41]. This transition depends on local symmetry and electric field around Dy^{3+} and this emission band depends strongly on the ligand environment. Whereas $^4F_{9/2}$ to $^6H_{15/2}$ (blue) transition at 484 nm due to magnetic dipole transition and follows the selection rules $\Delta L = 0$ and $\Delta J = 0, \pm 1$ [34,39–41]. These transitions are less sensitive to the local coordination

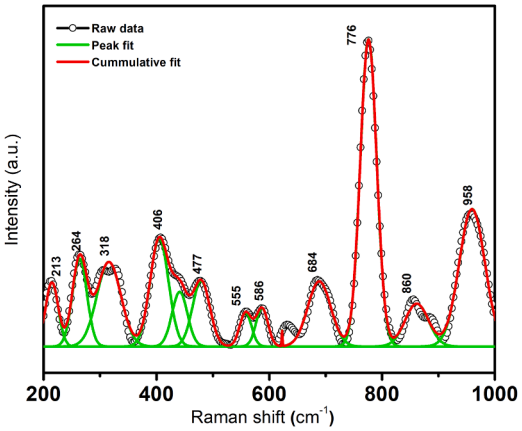

Fig. 8. Deconvoluted Raman spectra of BDAg glass system.

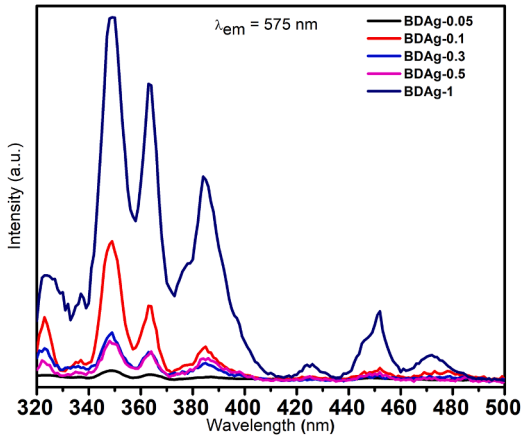

Fig. 9. Luminescence spectra (λ_{ex} = 575 nm) of BDAg glass system.

environment and the emission band at 484 nm is independent of local crystal field around Dy^{3+} ions in glass matrix in the BDAg host glass matrix. The high intensity of the emission band at 575 nm is stronger than the emission band at 484 nm due to Dy^{3+} ions positioned at locally sited low and high symmetries for yellow and blue emission respectively [34,39]. The PL features of Dy^{3+} doped BDAg glasses have been affected by network structures and locally sited symmetries of Dy^{3+} ions [26]. Intensity of the electron dipole transition has increased when the $Dy3^{+}$ ions interact strongly with its host matrices, which results in host matrix becomes more asymmetric in nature [34,39]. The electron dipole interaction is higher than the magnetic dipole transition in all synthesized BDAg glasses, this indicates that asymmetric nature of glasses. The wavelength corresponds to an intense emission bands that exhibit intense excitation spectra. Fig. 10 shows the photoluminescence excitation spectra of Ag concentration and doping with dysprosium ions of BDAg glass system in the wavelength of 320–500 nm by the emission wavelength of 575 nm. It was observed that eight distinct peaks at 323 nm, 337 nm, 349 nm, 363 nm, 384 nm, 425 nm, 452 nm and 472 nm correspond to [$^6H_{15/2}$ to $^4M_{17/2}$, $^6P_{3/2}$], [$^6H_{15/2}$ to $^4I_{9/2}$], [$^6H_{15/2}$ to $^6P_{7/2}$], [$^6H_{15/2}$ to $^4I_{11/2}$, $^6P_{5/2}$], [$^6H_{15/2}$ to $^4I_{13/2}$, $^4F_{7/2}$], [$^6H_{15/2}$ to $^4G_{11/2}$], [$^6H_{15/2}$ to $^4I_{15/2}$] and [$^6H_{15/2}$ to $^4F_{9/2}$] transitions of Dy^{3+} ions respectively [42]. It was observed that the position of the excitation bands has not considerably changed, however, the intensity of the bands has increased as an increase in the concentration of Ag from 0.05 to 1 mol% in Dy^{3+} doped BDAg glass matrix. The most intense excitation band was observed for $^6H_{15/2}$ to $^6P_{7/2}$ transition at 349 nm among all other bands, this wavelength corresponds to intense excitation band exhibits intense emission spectra [43].

The luminescence intensity of excitation and emission peaks as a function of Ag concentration were plotted and shown in Figs. 11 and 12 respectively. It was observed that the intensity of the peaks is increased as increase in the concentration of Ag from 0.05 to 0.1 mole% and then slightly decreased up to 0.3 mol%. Further the luminescence intensity has increased up to Ag concentration of 1 mol% in the Dy3+ doped BDAg glass matrix. The slight decrease of intensity of peaks from 0.05 to 0.3% of Ag could be due to the reverse energy transfer from Dy^{3+} ions to Ag nano particles. It is evident that the overall intensity of the peaks has increased as increase in the concentration of Ag.

It was reported in the literature that the high intensity emission bands are observed around 483 nm (blue) and 574 nm (yellow) corresponds to the $^4F_{9/2}\rightarrow{}^6H_{15/2}$ and $^4F_{9/2}\rightarrow{}^6H_{13/2}$ transitions respectively for Dy^{3+} doped borate glass matrix. Another small intensity band is observed around 665 nm (red). The intensity of emission spectra has increased up to 0.5 mol% of Dy^{3+} ions and then decreased. These Dy^{3+} doped borate glass system emits white light [38,44,45]. It is reported that the luminescence intensity ratios of Eu^{3+} and Dy^{3+} ions of red and yellow/blue emission values correspond to $^5D_0$–$^7F_2$/$^5D_0$–$^7F_1$ and

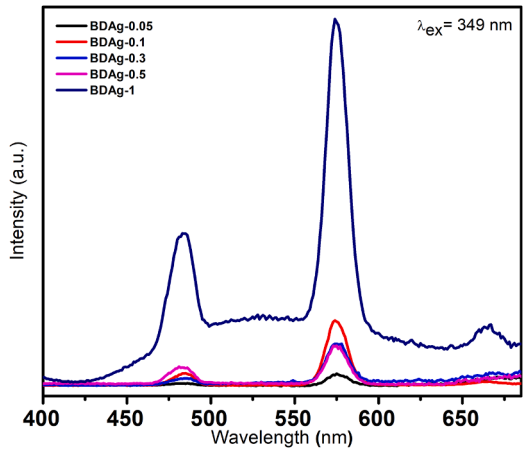

Fig. 10. Luminescence spectra (λ_{ex} = 349 nm) of BDAg glass system.

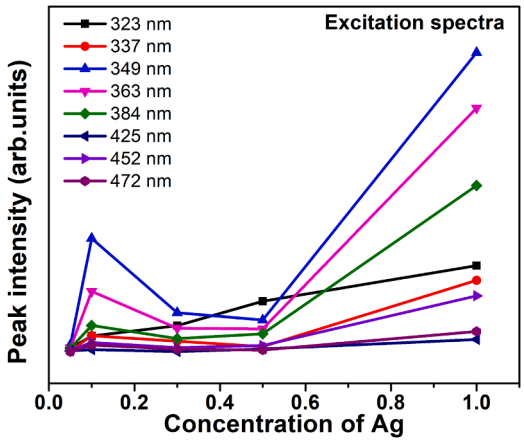

Fig. 11. Peak intensity as a function of Ag concentration of BDAg glass system.

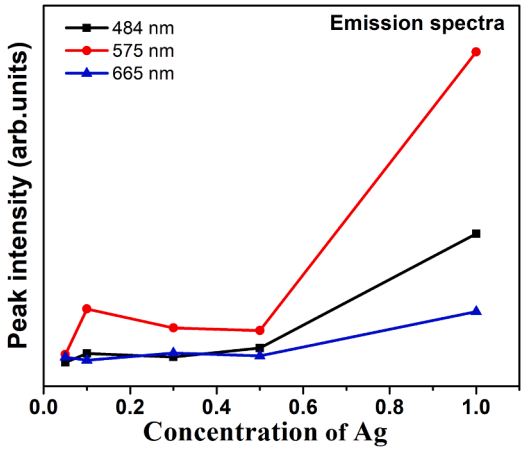

Fig. 12. Peak intensity as a function of Ag concentration of BDAg glass system.

$^4F_{9/2}$–$^6H_{15/2}$/$^4F_{9/2}$–$^6H_{13/2}$ transitions were increased as increase in the metallic content and this suggest that higher asymmetry and covalent bonding nature between the rare earth ions and oxygen ions. In the case of Pr^{3+} doped borate glass matrix, the high intense peak is observed at 663 nm due to energy transfer from to Pr^{3+} to Dy^{3+} [46]. The lifetime of the transitions was decreased when composition of glass varied and also contains modifier in the glass matrix. Observed decay curves are non-exponential for higher concentrations due to non-radiative energy transfer among excited Dy^{3+} ions [47]. Dy^{3+}/Tb^{3+}codoped glasses shown yellowish green regions as a function of the different concentrations Dy^{3+} with 350 and 395 nm excitation [48]. The emission probabilities from the $^4F_{9/2}\rightarrow{}^6H_{15/2}$ and $^4F_{9/2}\rightarrow{}^6H_{13/2}$ transitions were increased and their lifetimes were decreased by adding Na_2O to glass system[49]. On the other hand, lifetime of the $^4F_{9/2}$ level has increased as increase in temperature of glass matrix [49]. The average lifetime of Dy^{3+} was found to be about 2.95 ns and 4.94 ns for blue and yellow emission bands respectively [50]. At higher concentration of Dy^{3+}, quenching of luminescence intensity was observed and also found that dipole–dipole interactions between the Dy^{3+} ions in glass matrix [39]. It is reported that the Dy^{3+} ions have been located in the higher symmetrical ligand environments when the ratio of yellow to blue is low [51].

In our studies, concentration of 0.5% Dy^{3+} is fixed and varied the concentration of Ag in the BDAg glass matrix. The XRD measurements shows that prepared glass matrix has amorphous nature. BO_3 and BO_4 and several other functional groups also found by Raman and FTIR measurements. These findings are highly comparable and well matched

with reported research so far. The compositional analysis and their distribution in the glass matrix was performed by SEM and EDS analysis. SPR phenomena was observed in the UV–Vis absorption spectra and it was found that the intensity of SPR band is increased up to 0.3% of Ag and then decreased. The high intensity emission bands are observed around 483 nm (blue) and 574 nm (yellow) corresponds to the $^4F_{9/2}\rightarrow{}^6H_{15/2}$ and $^4F_{9/2}\rightarrow{}^6H_{13/2}$ transitions respectively for Dy^{3+} doped borate glass matrix. Small intensity band observed around 665 nm (red) correspond to $^4F_{9/2}$ to $^6H_{11/2}$ transition. Position of these emission bands is comparable and excellently matched with reported literature of Dy^{3+} doped borate glass matrix. It is found the intensity of these emission bands has increased as increase in the concentration of Ag in BDAg glass system. These results suggest that this BDAg glass system is very useful for white light emitting diodes.

5. Conclusions

In this study, the glasses with (60-x-y-z) B_2O_3 – 20 ZnO – 10 Na_2O – 10 Li_2O – xSnO – yDy_2O_3 – zAg_2O composition were prepared by conventional melt-quenching technique. The effect of formations of silver nano particles in Dy^{3+} doped glass system was investigated. The thermal stability factor was reported from the DSC thermogram. From DSC results, it is obvious that glass has greater thermal stability ΔT >100 °C which suggests that these glasses can be used as a prominent material for optical fibers. The optical absorption spectra showed four absorption bands with hypersensitive transition corresponding to $^6H_{15/2}$ to $^6F_{11/2}$ at 1260 nm. The band present at 420 nm explains the SPR phenomenon of BDAg glass system and a series of physical properties such as ion concentration, polaron radius, inter-nuclear distance, oscillator strength, energy bandgap, refractive index and other parameters are calculated for each composition of glass system. Interesting results of presence of BO_3 and BO_4 structural units were confirmed from FTIR and Raman spectroscopic studies. Photoluminescence measurements suggest that the Dy^{3+} doped glasses exhibit a strong yellow emission at 575 nm and other blue emission at 483 nm correspond to transitions of $^4F_{9/2}$ to $^6H_{13/2}$ and $^4F_{9/2}\rightarrow{}^6H_{13/2}$ due to electric dipole moment and magnetic dipole moment transitions respectively. In addition to that, the small intense emission band was observed for $^4F_{9/2}$ to $^6H_{11/2}$ at 665 nm (red). Observed results demonstrated that the luminescence properties of these glasses have been enhanced in the presence of silver nano particles. These results indicate that the prepared glasses can be widely used in solid state devices and lasers. It is also observed that the intensity of excitation bands has increased as increase in the concentration of Ag. The most intense excitation band was observed at 349 nm for $^6H_{15/2}$ to $^6P_{7/2}$ transition. These results indicate that the prepared glasses can be widely used in solid state devices and lasers.

CRediT authorship contribution statement

Ashok Ande: Conceptualization, Data curation, Formal analysis, Investigation, Methodology, Software, Writing - original draft, Writing - review & editing. **J. Bhemarajam:** Data curation. **Venkanna Kanneboina:** Formal analysis, Investigation, Writing - original draft, Writing - review & editing. **:** Writing - review & editing. **M. Prasad:** Supervision.

Declaration of Competing Interest

The authors declare that they have no known competing financial interests or personal relationships that could have appeared to influence the work reported in this paper.

References

[1] M.J.F. Digonnet, Rare-Earth-Doped Fiber Lasers and Amplifiers, CRC Press, 2001, 9780429207662, https://doi.org/10.1201/9780203904657. ISBN.

[2] P.N. Prasad, Nanophotonics, John Wiley & Sons, Inc., 2004. ISBN 0-471-64988-0.

[3] C. Strohhöfer, A. Polman, Silver as a sensitizer for erbium, Appl. Phys. Lett. 81 (2002) 1414–1416, https://doi.org/10.1063/1.1499509.

[4] G. Fu, W. Cai, C. Kan, C. Li, L. Zhang, Controllable optical properties of Au/SiO2 nanocomposite induced by ultrasonic irradiation and thermal annealing, Appl. Phys. Lett. 83 (2003) 36–38, https://doi.org/10.1063/1.1589190.

[5] L.P. Naranjo, C.B. De Araújo, O.L. Malta, P.A.S. Cruz, L.R.P. Kassab, Enhancement of Pr3+ luminescence in PbO- GeO2 glasses containing silver nanoparticles, Appl. Phys. Lett. 87 (2005) 1–3, https://doi.org/10.1063/1.2143135.

[6] H. Mertens, A. Polman, Plasmon-enhanced erbium luminescence, Appl. Phys. Lett. 89 (2006), 211107, https://doi.org/10.1063/1.2392827.

[7] Y. Hamanaka, A. Nakamura, S. Omi, N. Del Fatti, F. Vallée, C. Flytzanis, Ultrafast response of nonlinear refractive index of silver nanocrystals embedded in glass, Appl. Phys. Lett. 75 (1999) 1712–1714, https://doi.org/10.1063/1.124798.

[8] S. Qu, C. Zhao, X. Jiang, G. Fang, Y. Gao, H. Zeng, Y. Song, J. Qiu, C. Zhu, K. Hirao, Optical nonlinearities of space selectively precipitated Au nanoparticles inside glasses, Chem. Phys. Lett. 368 (2003) 352–358, https://doi.org/10.1016/S0009-2614(02)01885-7.

[9] M. Yamane, Y. Asahara, Glasses for Photonics, Cambridge University Press, 2000, https://doi.org/10.1017/CBO9780511541308. ISBN 0-511-03862-3.

[10] C.H. Kam, S. Buddhudu, Near infrared to red and yellow to blue upconversion emissions from Pr3+: zrF4-BaF2-LaF3 -YF3-AlF3-NaF glasses, J. Quant. Spectrosc. Radiat. Transf. 85 (2004) 1–12, https://doi.org/10.1016/S0022-4073(03)00190-0.

[11] C.H. Kam, S. Buddhudu, Emission analysis of Eu3+:bi2O3- B2O3-R2O (R=Li,Na,K) glasses, J. Quant. Spectrosc. Radiat. Transf. 87 (2004) 325–337, https://doi.org/10.1016/j.jqsrt.2004.03.006.

[12] Z. Dai, A. Fang, Theory of Pr3+:ZBLAN ultraviolet upconversion fiber master oscillator power amplifier, J. Quant. Spectrosc. Radiat. Transf. 101 (2006) 226–236, https://doi.org/10.1016/j.jqsrt.2005.11.016.

[13] T.Y. Lim, H. Wagiran, R. Hussin, S. Hashim, M.A. Saeed, Physical and optical properties of dysprosium ion doped strontium borate glasses, Phys. B Condens. Matter. 451 (2014) 63–67, https://doi.org/10.1016/j.physb.2014.06.028.

[14] M. Subhadra, P. Kistaiah, Infrared and Raman spectroscopic studies of alkali bismuth borate glasses: evidence of mixed alkali effect, Vib. Spectrosc. 62 (2012) 23–27, https://doi.org/10.1016/j.vibspec.2012.07.001.

[15] Z. Mu, Y. Hu, L. Chen, X. Wang, Enhanced luminescence of Dy3+ in Y3Al 5O12 by Bi3+ co-doping, J. Lumin. 131 (2011) 1687–1691, https://doi.org/10.1016/j.jlumin.2011.03.072.

[16] M. Fleischmann, P.J. Hendra, A.J. McQuillan, Raman spectra of pyridine adsorbed at a silver electrode, Chem. Phys. Lett. 26 (1974) 163–166, https://doi.org/10.1016/0009-2614(74)85388-1.

[17] D.A. Weitz, S. Garoff, J.I. Gersten, A. Nitzan, The enhancement of Raman scattering, resonance Raman scattering, and fluorescence from molecules adsorbed on a rough silver surface, J. Chem. Phys. 78 (1983) 5324–5338, https://doi.org/10.1063/1.445486.

[18] E. Snoeks, A. Lagendijk, A. Polman, Measuring and modifying the spontaneous emission rate of erbium near an interface, Phys. Rev. Lett. 74 (1995) 2459–2462, https://doi.org/10.1103/PhysRevLett.74.2459.

[19] G.M. Kumar, D.N. Rao, G.S. Agarwal, Experimental studies of spontaneous emission from dopants in an absorbing dielectric, Opt. Lett. 30 (2005) 732, https://doi.org/10.1364/ol.30.000732.

[20] G.M. Kumar, D.N. Rao, G.S. Agarwal, Measurement of local field effects of the host on the lifetimes of embedded emitters, Phys. Rev. Lett. 91 (2003) 1–4, https://doi.org/10.1103/PhysRevLett.91.203903.

[21] R.S.E.S. Dawaud, S. Hashim, Y.S.M. Alajerami, M.H.A. Mhareb, N. Tamchek, Optical and structural properties of lithium sodium borate glasses doped Dy3+ ions, J. Mol. Struct. 1075 (2014) 113–117, https://doi.org/10.1016/j.molstruc.2014.06.032.

[22] B. Meyer, F. Borsa, S.W. Martin, Structure and properties of lithium thio-borogermanate glasses, J. Non. Cryst. Solids. 337 (2004) 166–173, https://doi.org/10.1016/j.jnoncrysol.2004.03.116.

[23] F. Urbach, The long-wavelength edge of photographic sensitivity and of the electronic Absorption of Solids, Phys. Rev. 92 (1953) 1324, https://doi.org/10.1103/PhysRev.92.1324.

[24] E.A. Davis, N.F. Mott, Conduction In Non-crystalline Systems .V. Conductivity, Optical Absorption and Photoconductivity In Amorphous Semiconductors, Philos. Mag. 22 (1970) 903–922, https://doi.org/10.1080/14786437008221061.

[25] V. Dimitrov, S. Sakka, Electronic oxide polarizability and optical basicity of simple oxides. I, J. Appl. Phys. 79 (1996) 1736–1740, https://doi.org/10.1063/1.360962.

[26] M.H.A. Mhareb, S. Hashim, A.S. Sharbirin, Y.S.M. Alajerami, R.S.E.S. Dawaud, N. Tamchek, Physical and optical properties of Li2O-MgO-B2O3 doped with Dy3+, Opt. Spectrosc. (English Transl. Opt. i Spektrosk. 117 (2014) 552–559, https://doi.org/10.1134/S0030400X14100166.

[27] Y.R.M. Parandamaiah, K. Naveen Kumar, S. Babu, S. Venkatramana Reddy, Dy3+ doped lithium sodium bismuth borate glasses for yellow luminescent photonic applications, J. Eng. Res. Appl. 5 (2015) 126–131. www.ijera.com.

[28] V.A.G. Rivera, S.P.A. Osorio, Y. Ledemi, D. Manzani, Y. Messaddeq, L.A.O. Nunes, E. Marega Jr., Localized surface plasmon resonance interaction with Er^3+-doped tellurite glass, Opt. Express. 18 (2010) 25321, https://doi.org/10.1364/oe.18.025321.

[29] M.Reza Dousti, M.R. Sahar, S.K. Ghoshal, R.J. Amjad, A.R. Samavati, Effect of AgCl on spectroscopic properties of erbium doped zinc tellurite glass, J. Mol. Struct. 1035 (2013) 6–12, https://doi.org/10.1016/j.molstruc.2012.09.023.

[30] T. Sekiya, N. Mochida, A. Ohtsuka, A. Soejima, Raman spectra of BO3 2TeO2 glasses, J. Non. Cryst. Solids. 151 (1992) 222–228, https://doi.org/10.1016/0022-3093(92)90033-G.

[31] A.M. Babu, B.C. Jamalaiah, J.S. Kumar, T. Sasikala, L.R. Moorthy, Spectroscopic and photoluminescence properties of Dy3+-doped lead tungsten tellurite glasses for laser materials, J. Alloys Compd. 509 (2011) 457–462, https://doi.org/10.1016/j.jallcom.2010.09.058.
[32] Y. Tian, R. Xu, L. Hu, J. Zhang, Broadband 2.84 μm luminescence properties and JuddOfelt analysis in Dy3 doped ZrF4BaF2LaF3AlF 3YF3 glass, J. Lumin. 132 (2012) 128–131, https://doi.org/10.1016/j.jlumin.2011.08.017.
[33] M.R. Dousti, M.R. Sahar, M.S. Rohani, A. Samavati, Z.A. Mahraz, R.J. Amjad, A. Awang, R. Arifin, Nano-silver enhanced luminescence of Eu3+-doped lead tellurite glass, J. Mol. Struct. 1065–1066 (2014) 39–42, https://doi.org/10.1016/j.molstruc.2014.02.032.
[34] K. Venkata Rao, S. Babu, G. Venkataiah, Y.C. Ratnakaram, Optical spectroscopy of Dy3+ doped borate glasses for luminescence applications, J. Mol. Struct. 1094 (2015) 274–280, https://doi.org/10.1016/j.molstruc.2015.04.015.
[35] I. Abdullahi, S. Hashim, S.K. Ghoshal, A.U. Ahmad, Structures and spectroscopic characteristics of barium-sulfur-telluro-borate glasses: role of Sm3+ and Dy3+ Co-activation, Mater. Chem. Phys. 247 (2020), 122862, https://doi.org/10.1016/j.matchemphys.2020.122862.
[36] A. Ashok, V. Vamsipriya, G. Upendar, M. Prasad, Optical and structural studies of B2O3–ZnO–Na2O–Li2O glasses containing Ag nano particles, Glas. Phys. Chem. 46 (2020) 378–388, https://doi.org/10.1134/S1087659620050028.
[37] R.Y. Parandamaiah M., K. Naveen Kumar, S. Babu, S. Venkatramana Reddy, Dy3+ doped lithium sodium bismuth borate glasses for yellow luminescent photonic applications, Int. J. Eng. Res. Appl. 5 (2015) 126–131. %0D.
[38] S. Damodaraiah, V. Reddy Prasad, S. Babu, Y.C. Ratnakaram, Structural and luminescence properties of Dy3+ doped bismuth phosphate glasses for greenish yellow light applications, Opt. Mater. (Amst). 67 (2017) 14–24, https://doi.org/10.1016/j.optmat.2017.03.023.
[39] B. Shanmugavelu, V.V.R.K. Kumar, Luminescence studies of Dy3+ doped bismuth zinc borate glasses, J. Lumin. 146 (2014) 358–363, https://doi.org/10.1016/j.jlumin.2013.10.018.
[40] O.B. Aljewaw, M.K.A. Karim, H.M. Kamari, M.H.M. Zaid, N.M. Noor, I.N.C. Isa, M. H.A. Mhareb, Impact of dy2o3 substitution on the physical, structural and optical properties of lithium–aluminium–borate glass system, Appl. Sci. 10 (2020) 1–17, https://doi.org/10.3390/app10228183.
[41] I. Khan, G. Rooh, R. Rajaramakrishna, N. Srisittipokakun, H.J. Kim, J. Kaewkhao, Y. Ruangtaweep, Photoluminescence properties of Dy3+ ion-doped Li2O-PbO-Gd2O3-SiO2 glasses for white light application, Braz. J. Phys. 49 (2019) 605–614, https://doi.org/10.1007/s13538-019-00695-0.
[42] M.V. Vijaya Kumar, B.C. Jamalaiah, K. Rama Gopal, R.R. Reddy, Optical absorption and fluorescence studies of Dy3-doped lead telluroborate glasses, J. Lumin. 132 (2012) 86–90, https://doi.org/10.1016/j.jlumin.2011.07.021.
[43] M.V.S. Kumar, D. Rajesh, A. Balakrishna, Y.C. Ratnakaram, Optical absorption and photoluminescence properties of Dy3+ doped heavy metal borate glasses - Effect of modifier oxides, J. Mol. Struct. 1041 (2013) 100–105, https://doi.org/10.1016/j.molstruc.2013.03.009.
[44] D. Rajesh, Y.C. Ratnakaram, M. Seshadri, A. Balakrishna, T. Satya Krishna, Structural and luminescence properties of Dy 3+ ion in strontium lithium bismuth borate glasses, J. Lumin. 132 (2012) 841–849, https://doi.org/10.1016/j.jlumin.2011.08.050.
[45] P.P. Pawar, S.R. Munishwar, S. Gautam, R.S. Gedam, Physical, thermal, structural and optical properties of Dy3+ doped lithium alumino-borate glasses for bright W-LED, J. Lumin. 183 (2017) 79–88, https://doi.org/10.1016/j.jlumin.2016.11.027.
[46] P.P. Pawar, S.R. Munishwar, R.S. Gedam, Physical and optical properties of Dy3+/Pr3+ Co-doped lithium borate glasses for W-LED, J. Alloys Compd. 660 (2016) 347–355, https://doi.org/10.1016/j.jallcom.2015.11.087.
[47] C.K. Jayasankar, V. Venkatramu, S.S. Babu, P. Babu, Luminescence properties of Dy3+ ions in a variety of borate and fluoroborate glasses containing lithium, zinc, and lead, J. Alloys Compd. 374 (2004) 22–26, https://doi.org/10.1016/j.jallcom.2003.11.051.
[48] G. Lakshminarayana, K.M. Kaky, S.O. Baki, A. Lira, U. Caldiño, I.V. Kityk, M. A. Mahdi, Optical absorption, luminescence, and energy transfer processes studies for Dy3+/Tb3+-codoped borate glasses for solid-state lighting applications, Opt. Mater. (Amst). 72 (2017) 380–391, https://doi.org/10.1016/j.optmat.2017.06.030.
[49] N.S. S.Tanabe a, J. Kang, T. Hanada, Yellow/blue luminescences of Dy 3+ doped borate glasses and their anomalous temperature variations, J. Non. Cryst. Solids. 239 (1998) 170–175.
[50] P.P. Pawar, S.R. Munishwar, R.S. Gedam, Intense white light luminescent Dy3+ doped lithium borate glasses for W-LED: a correlation between physical, thermal, structural and optical properties, Solid State Sci. 64 (2017) 41–50, https://doi.org/10.1016/j.solidstatesciences.2016.12.009.
[51] R. Vijayakumar, R. Nagaraj, P. Suthanthirakumar, P. Karthikeyan, K. Marimuthu, Silver (Ag) nanoparticles enhanced luminescence properties of Dy3+ ions in borotellurite glasses for white light applications, Spectrochim. Acta - Part A Mol. Biomol. Spectrosc. 204 (2018) 537–547, https://doi.org/10.1016/j.saa.2018.06.092.